Thermally induced non-linear vibration of single-walled carbon nanotubes

Heeyuen Koh, James J. Cannon, Takuma Shiga, Junichiro Shiomi, Shohei Chiashi and Shigeo Maruyama*

Department of Mechanical Engineering, The University of Tokyo, 7-3-1 Hongo, Bunkyo-ku, Tokyo 113-8656, Japan

Keyword: Single-walled carbon nanotubes, Non-linear thermal vibration, Molecular dynamics, Continuum mechanics, Green-Lagrange strain tensor, Galerkin method

PACs: 61.48.De, 85.35.Kt, 63.22.Gh, 65.80.-g

Abstract

The thermally induced nonlinear vibration of single-walled carbon nanotubes (SWNT) was investigated, focusing on the peak broadening and/or multiple peaks of the frequency spectra. From Poincaré maps of SWNT tip trajectories, we observed two distinguishable patterns of vibration: planar and non-planar (whirling) motion which appeared repeatedly. The alternation of the pattern is sometimes accompanied by a change of rotational direction. Proposed approximate solutions of non-linear beam equations can reproduce well the alternation of the patterns for both cantilevered and suspended SWNTs. By using this analytical approach, we have found that multiple peaks of experimentally observed frequency spectra are due to the repeated and sudden alternations of 2 modes, induced by non-linear effects.

1. Introduction

Mechanical resonators used for mass and force sensors or quantum optomechanical system have drastically improved their quality factors (Q factors), by using nanoscale materials [1-4], because of the ultra-low-mass and highly elastic features. Carbon nanotube field effect transistors (FET) are the most studied configuration of mechanical resonators [1-2, 4-8]. In order to address the upper-bound of the Q-factor, the physical mechanism of peak broadening and multiple peaks in frequency spectra have been discussed based on several cryostat temperature measurements [1,2,5] and phonon collision theories [9]. The range of the Q factor and the experimental condition which decides the Q factor, will become increasingly important in order to expand the boundaries of applications using nano scale resonators at room temperature.

In many experiments, the framework of continuum mechanics [10-12] has been employed for elastic modulus and Q factor from the bending motion of SWNT [13-17]. Recent state-of-the-art experimental reports are employing suspended single-walled carbon nanotubes (SWNT) such as mixers [6,18] and sensors [1-2,19-22], including pioneering research on the motion of wave guides [23] and quantum theory on macroscopic motion of a SWNT [24], which are related to the low frequency transverse mode.

While the remarkable properties of carbon nanotubes (CNT) have been applied in experiments, the theory to describe its continuum like behavior (i.e. bending) has also been improved from the well-known Cauchy-Born rule to describe the relation between continuum mechanics and solid state physics systems [25-27]. The characteristics of dynamics such as frequency response of transverse mode, are also shown to have a good agreement with continuum bar theories for SWNT and statistical mechanics using MD simulations [28, 29].

One further step would be to reconcile the remaining discrepancies such as the limits of continuum bar models, where the peak broadening process is based on the dissipation of

vibration energy until the kinetic energy reaches to zero, unlike molecular systems which retain thermally induced vibration after dissipation. Recent experiment and theories on the response of SWNT [6,30,31] or graphene [32] with forced excitation, have suggested the existence of nonlinear damping, which emerges with multiple peaks in the frequency domain. In this case, it is difficult to apply the conventional Lorentzian fitting for Q factor.

The multiple peaks in the frequency response indicate that the signal from the displacement of SWNT's motion has beating signals. This means that the macroscopic motion from the transverse mode should result in irregular amplitude in the time domain. Nonlinearity of macroscopic motion like "jumping rope" or "whirling motion" [33, 34] can be one possible way to produce a beating signal like the motion reported in nonlinear vibration of a continuum rod from mode coupling experiment [35]. Considering the similarity between a molecular system and continuum bar theories, nonlinear mode coupling analysis can be a reasonable approach to try.

To explore the limit of continuum frameworks for frequency response for the first transverse mode in a tubular system, especially for its multiple resonance peaks in FET systems, the free thermal vibration of various SWNTs without any external forces is calculated using MD simulation so that we can exclude the effect of the dissipative coupling [36]. Several SWNTs are calculated with different temperatures. Most of them show nonlinear behavior periodically. This provides an interesting point of view for multiple resonance peaks in experimental results.

2. Simulations and analytical technique

2-1 Molecular dynamics simulations

Armchair and zigzag SWNTs are observed during free thermal vibration. (5,5), (10,10),

(10,0), (20,0) and (20,20) SWNTs are prepared with various length of 5 nm ~ 25 nm. We employed the adaptive intermolecular reactive bond order (AIREBO) potential function [37] to describe the carbon-carbon interaction using the LAMMPS package [38] including the torsion. Simulations are performed over 20 ns time span at 50, 100 and 300 K. The integration time step size is 0.5 fs. A Langevin thermostat [39] is used with a damping coefficient of 0.01 ps. The calculation with a Nose-Hoover thermostat [40] did not alter the result significantly. After energy-minimization, a thermostat is employed for 1 ns and there is another 1 ns simulation under an NVE ensemble condition before data collection. To realize the fixed boundary condition, the Lennard-Jones (12-6) potential was used for each carbon atom at the end of SWNT [41,42]. The coefficients of this potential, ϵ_{LJ} and σ, are 20 eV and 0.8909 Å, respectively. Three more different boundary coefficients are examined for the effect of the rigidity on the motion. A schematic figure of the simulation system used in this work is depicted in Fig. 1 and an image of the artificial boundary condition is shown in Fig. 2. The specific conditions for simulation models with various aspect ratios are in Table 1 and other conditions are in Table S2~S6 of Supporting Material B [43].

Table 1. Simulation conditions with various aspect ratios.

	R (nm)	Num. of Atoms	L (nm)	Temp. (K)
(5,5)	0.34	400	4.28	50/100/300
		480	5.58	
		560	6.56	
		660	7.6	
		820	9.8	
		1620	19.8	
(10,10)	0.667	1320	7.6	
		4000	25.3	
(20,20)	1.36	8000	25.3	

2-2 Approximate analytical solution

The jumping rope motion as shown in Fig 1(b) has been suggested as the reason of multiple peaks in the frequency domain by inducing the degeneration mode between two orthogonal axes [33, 34] in suspended FET systems. Forced excitation was considered but the parameter match for SWNT with dissipation coupling has shown some limits [34]. Therefore, starting from analytical solution for free vibration (free thermal vibration) can be a good initial step towards unknown dissipation mechanism.

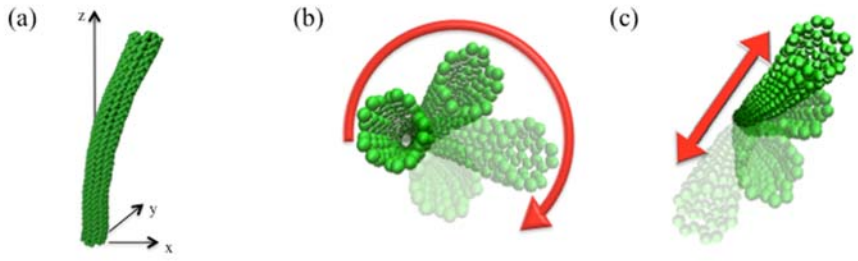

Fig. 1. Visualization of motion from MD simulation. The averaged coordinate of each carbon ring perpendicular to tube axis is amplified 5 times to clearly visualize the motion: (a) schematic figure of system, (b) non planar motion, (c) planar motion.

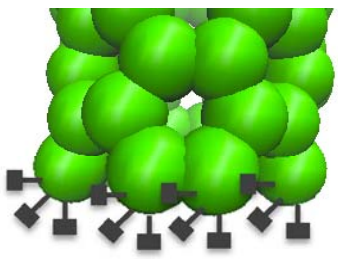

Fig. 2 Fixed boundary using LJ potential spring. Each atom has 3 springs along cartesian axis and the force is calculated using LJ potential function with the coefficients are in Table S2 in Supporting Material B.

The equation of the motion of bending using the strain energy to couple the bending motion in two orthogonal axes for free vibration is derived by Ho [44]:

$$u_{\tau\tau} + \frac{I}{AL^2}\left(u_{ssss} - \beta\pi^2 u_{ss}\right) - \frac{1}{2}u_{ss}\int_0^1 \left(u_s^2 + v_s^2\right)ds = 0 \tag{1}$$

$$v_{\tau\tau} + \frac{I}{AL^2}\left(v_{ssss} - \beta\pi^2 v_{ss}\right) - \frac{1}{2}v_{ss}\int_0^1 \left(u_s^2 + v_s^2\right)ds = 0 \tag{2}$$

where, u, v are non-dimensionalized displacements along x, y axis and s is the length along the tube axis. All of them are non-dimensionalized by L, the total length of the tube. τ is the non-dimensionalized time which is equal to the time *t* multiplied with $\frac{1}{L}\sqrt{\frac{E}{\rho}}$. E is Young's modulus and ρ is the aerial density of the tube; here, we use the density of graphene. β is $AL^2\varepsilon_0 / I\pi^2$ and ε_0 is the thermal expansion coefficient. I represents the momentum of inertia.

An analytical solution to this nonlinear bending equation has been described only for a suspended bar structure [44]. Here, the displacements along x and y axis for cantilevered boundary case are assumed to be $u = \xi(\tau)\sin(\pi s/2)$ and $v = \eta(\tau)\sin(\pi s/2)$ instead of $u = \xi(\tau)\sin(\pi s)$ and $v = \eta(\tau)\sin(\pi s)$ as for the suspended condition. It is supposed that the displacement caused by the 1st transverse mode is very large so that the higher frequency modes terms are ignored. Because of the higher order terms in governing equations, the amplitude of tip excursion, $\xi(\tau)$ and $\eta(\tau)$ are supposed as the combination of two time-varying variables as $\xi(\tau) \cong a(\tau)\cos(\omega\tau + \theta(\tau))$ and $\eta(\tau) \cong b(\tau)\sin(\omega\tau + \phi(\tau))$. Solving the analytical solution of Eq. (1)~(2) for the cantilevered condition is a matter of changing the physical interpretation of the pre-strain ϵ_0 to the thermal expansion coefficient, which is the constant from the integration.

Substituting these definitions into the governing equation, the approximate solutions are derived to be the same as derived by Ho [44]:

$$a^2(\tau) = \frac{c_1^2}{2} + \frac{c_1^2}{2}\sqrt{1-C_0^2}\sin\left(\frac{qc_1^2}{4\omega}C_0\tau\right), \tag{3}$$

$$b^2(\tau) = \frac{c_1^2}{2} - \frac{c_1^2}{2}\sqrt{1-C_0^2}\sin\left(\frac{qc_1^2}{4\omega}C_0\tau\right), \tag{4}$$

$$\theta(\tau) = \left(\frac{3qc_1^2}{8\omega}+\Gamma\right)\tau - \tan^{-1}\left(\frac{\sqrt{1-C_0^2}}{C_0} + \frac{1}{C_0}\tan\frac{qC_0c_1^2}{4\omega}\tau\right), \tag{5}$$

$$\phi(\tau) = \left(\frac{3qc_1^2}{8\omega}+\Gamma\right)\tau - \tan^{-1}\left(-\frac{\sqrt{1-C_0^2}}{C_0} + \frac{1}{C_0}\tan\frac{qC_0c_1^2}{4\omega}\tau\right), \tag{6}$$

$\Gamma = \varepsilon_0\pi^2/4$ and A is cross-sectional area. q is a constant $\pi^2/64$ for this case and $\pi^2/4$ for suspended case. The differences in the analytical solutions for cantilevered and suspended SWNT's are the value of q and the natural frequency which should be the non-dimensional constant ω defined as $\pi^2/4\sqrt{I/AL^2}$ for cantilevered and $\pi^2\sqrt{I/AL^2}$ for suspended SWNTs. Here, we use 0.0706 nm as the thickness of each SWNT in order to decide I consistent with continuum tube model [16]. Excluding parameters from the initial condition which show negligible influence, there are 3 essential unknowns left; Γ, C_0 and c_1. The initial condition parameters from integration are simply ignored after their influence to the results manually. c_1 is the maximum amplitude of 1 st transverse mode measured from the origin. C_0 is the parameter for adjusting the interaction rate between the displacement along x and y axis.

3. Nonlinear behaviour of SWNT

The motion of bending in cantilevered and suspended SWNT is observed using a Poincaré map and the angular velocity profile. The poincaré map presents the trajectory of the tip location of SWNT during certain time span, and the angular velocity is attained from the azimuth angle of tip location from the origin. The schematic figure of measuring the azimuth angle of the tip is shown in Fig 3.

More precisely, the difference of the angle with 5 fs time span is measured and divided with this sampling time to calculate angular velocity of the tip. The positive value of angular velocity means that the tip is drawing the trajectory in clock-wise or vice versa.

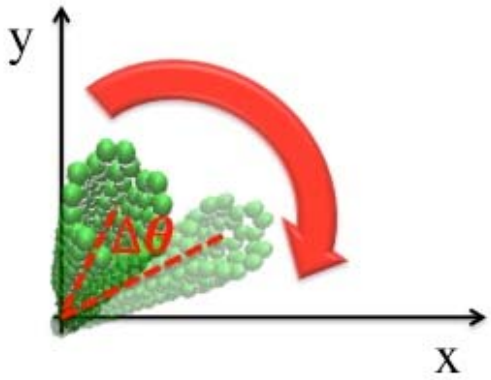

Fig. 3 Schematic figure to measure the rotation exchange.

3-1.Planar and non-planar motion from Poincaré map

The poincaré map directly shows the shape of motion; planar or non-planar. Planar motion is typical harmonic bending motion in a plane. Non-planar motion means the tube is whirling like a jumping rope. Fig. 1 (b) and (c) show the planar and non-planar motion caused by free thermal vibration in MD simulation. The motion repeatedly switches its trajectory shape between planar and non-planar motion as shown the movie in Supporting Material A [43]. The exchange between the two different types of motion means that the free thermal vibration has highly nonlinear characteristics. The typical exchange is well presented in Fig. 4 (1)~(6). Similar trend is equally observed in the suspended cases.

For the trajectory of the tip, the displacement of a half of unit cell is averaged. In case of cantilevered, a ring under a unit cell at the unfixed end of tube is chosen and a cell at the center of tube is picked for suspended SWNT. The sampling frequency is 5 fs for both conditions. Since the observation is focused on the motion caused by the 1st transverse vibration mode in SWNT, the averaged displacement data is processed with filtering to eliminate the influence of the higher order modes shown in Fig. 4 (a)~(f). The square window is used and the cut off frequency employed is 50 GHz, which is higher than the resonance frequency about 44 GHz. The shape of motion gradually changes from planar to non-planar. A rapid change of the rotation direction is observed during the non-planar motion, which can be recognized with the angular velocity profile in Fig. 5 and Fig. 6.

Using the analytical solutions, we tried to reproduce the smoothed MD result. The 3 unknown parameters in Sec 2 are determined as explained in Sec 3-3. According to Eq. (3)~(6), planar and non-planar motion with rotational direction inversion should appear repeatedly. How often this inversion occurs is dependent on the amplitude of the motion, c_1 with the adjustment parameter, C_0. The Poincaré map from the fitted results in Fig. 4 (i) ~(vi) as well as the Movie in Supporting Material A [43] display striking agreement between the results from MD simulation and the analytical solution. In case of zigzag SWNT, the same trend appears but its result is not included in the fitting process in this paper.

3-2. Inversion of rotional direction from angular velocity profile

The angular velocity of the tip gives the information regarding to the reverse of rotational direction and the exchange between planar and non planar motion, simultaneously. The rotation of the tip typically records high angular velocity, e.g. 6 *rad/ps* during the planar motion as shown in Fig. 5, because of its trajectory shape near the origin. The planar motion in MD simulation in Fig. 4 (b) and analytic solution as Fig. 4 (ii) are not perfectly in a line so

that the trajectory draws very narrow eclipse. Besides, in case of MD, the direction of rotation can be easily flipped to the opposite direction during planar motion so the sign of angular velocity results in noisy profile as shown in 5~8 ns range in Fig. 5 (c). These may occur due to the instability of the motion against mode interaction with higher modes, which has small wave length. This kind of noise is ignored in Fig 6 (a) during the comparison with the analytical solution. In case of non planar motion, the angular velocity remains as constant as shown in Fig. 5 (a). It is observed that the rotational direction of non-planar motion is occasionally inversed from clockwise to counter clockwise and vice versa. This condition is separately named as 'transient' mode. This can be confirmed using the angular velocity profile in Fig. 5 (b) and (c), most of the simulation models show more rotation inversion at higher temperature.

The arrows in Fig. 6 correspond to each Poincaré maps in Fig. 4. The sequence of the motion exchange of planar and non-planar is well reproduced by the analytical approach. We confirmed that the similar agreement in all other SWNTs with different aspect ratio including suspended case. Zig-zag and chiral tubes are also examined and showed same nonlinearity but the fitting result are not included in this paper.

3-3 Parameter fitting process

Each unknown parameter in Eq. (3)~(6) is fitted with the following methods.

The Gibbs-Boltzmann distribution for elastic wave modes, $Z^{-1}e^{-KU^2/(2k_BT)}$ is adapted [28] where the ensemble average, $\left\langle U^2 \right\rangle = \left\langle c_1^2 L^2 \right\rangle = k_B T / K$. $K = 3EI / L^3$ is a spring constant and U is the maximum displacement of the 1st transverse vibration according to the Gibbs-Boltzmann distribution. Young's modulus, E to calculate spring constant is from the empirical formulation [46] for initial guess and gives reasonable range of c_1. This approximation is not as precise for short SWNTs, which is not in the Euler beam range. The

value for each simulation model is presented in Supporting Material B [43].

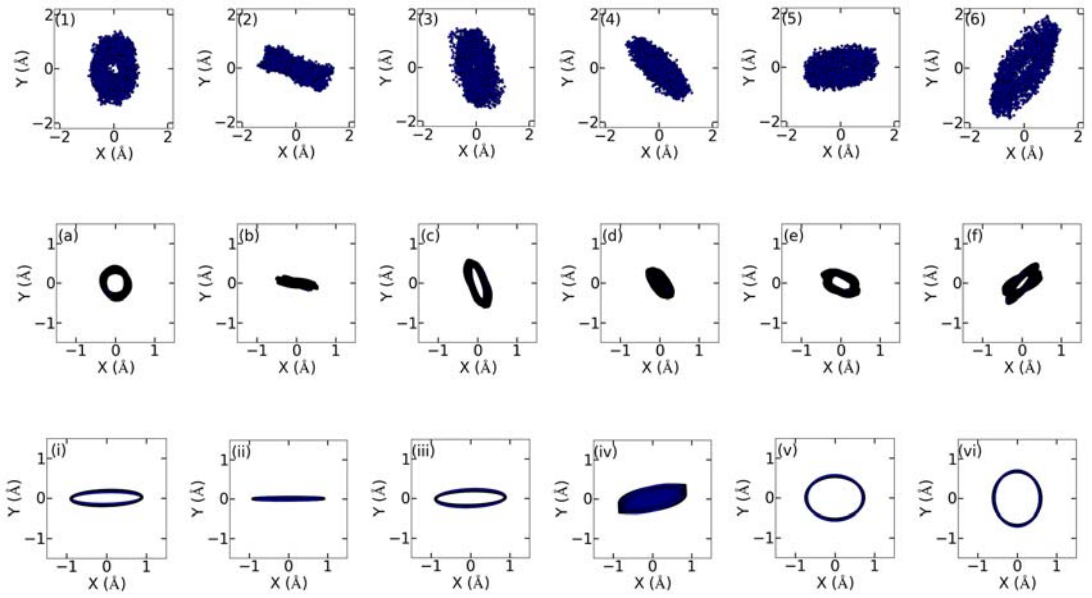

Fig. 4. Poincaré map of (5,5) SWNT with 7.6 nm length at 300 K from MD (1~8), low pass filtered result (a~h) and analytical solution (i~viii); (1) 2.5 ~ 3 ns, (2) 6.5 ~ 7 ns, (3) 10 ~ 10.5 ns, (4) 15 ~ 15.5 ns, (5) 19 ~ 19.5 ns, (6) 22.5 ~ 23 ns in MD; (a) 2.5 ~ 3 ns, (b) 6.5 ~ 7 ns, (c) 10 ~ 10.5 ns, (d) 15 ~ 15.5 ns, (f) 22.5 ~ 23 ns in low-pass filtered; (i) 2.5 ~ 3 ns , (ii) 6.5 ~ 7 ns, (iii) 10 ~ 10.5 ns, (iv) 15 ~ 15.5 ns, (v) 19 ~ 19.5 ns, (vi) 22.5 ~ 23 ns in alaytical solution.

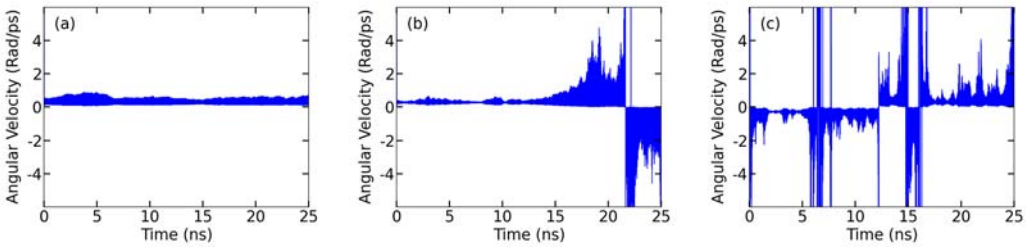

Fig. 5. Angle velocity plots by MD for (5,5) SWNT 7.6 nm; (a) 50 K, (b) 100 K, (c) 300 K.

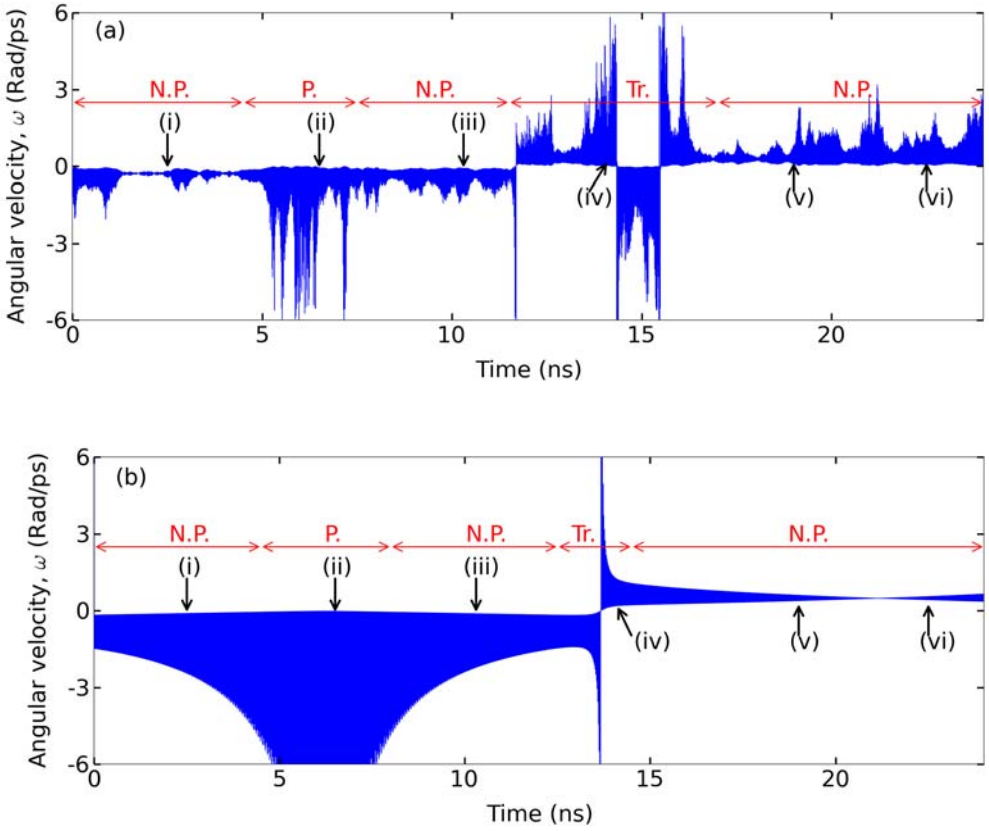

Fig. 6. Comparison of motion type exchange in Poincaré map, N.P. and P. indicate non-planar and planar. Tr. is transient period to inverse the rotational direction; (a) MD simulation and (b) analytical solution, The motion at (i)~(vi) is compared in Fig. 4.

C_0 can be considered after c_1 is determined. The constant C_0 is the parameter for adjusting the rate of exchange of planar and non-planar motion and the inversion of rotational direction. The changing ratio is decided from $\frac{qc_1^2}{4\omega}C_0$ and $\frac{qc_1^2}{2\omega}C_0$ for the exchange of motion type and the inversion of rotational direction respectively, according to Eq. (3)~(6). The value of C_0 for each simulation is decided by matching the Poincaré map and angular velocity profile of analytic solution to that of MD simulation result. Because the time variable, τ, in the analytic solution is non-dimensionalized by $\frac{1}{L}\sqrt{\frac{E}{\rho}}$, the number of cycle of 1st mode motion is counted from MD data so that the exchange of motion type and rotation inversion

of analytic solution can be occurred during the same number of cycles. The Young's modulus in $\frac{1}{L}\sqrt{\frac{E}{\rho}}$ is decided by later matching the peak location in the frequency domain, once more but there was no significant difference.

The thermal expansion coefficient Γ, which is Gruneissen parameter [48] multiplied with $\pi^2/4$, plays a role in the frequency shift. Its influence on whirling motion, however, is negligible and the location of peaks adjusts mainly with time constant from Young's modulus so that The simple thermal expansion averaged from tube axial distribution is used. The variation of the Young's modulus, however, is very narrow so it is maintained as a constant in most of cases. The value of each parameter is in Table 2 and Supporting Material B [43].

4. Physical meaning of nonlinear motion

4-1. Comparison in frequency domain

Fitted results of the analytical solution for (5,5) 7.6 length are compared with MD simulation in frequency domain in Fig. 7. The peak shapes in frequency domain correspond well with the fitted analytic solution. The displacement of the tip at high temperature has more frequent exchanges of the type of motion and rotational direction, so that the signal has more beating, which induces the separation of peak clearer instead the peak width becoming larger.

Another interesting point is that the frequency shift by temperature is well described by the analytical solution. Such frequency shift dependence on temperature is well reported in another MD simulation paper [31]. Eq. (5) ~ Eq. (6) make such trend by the phase dependent on amplitude. Higher temperature cases have a somewhat different trend. This is discussed in Section 4-5. The slight difference in the value of Young's modulus for each temperature

condition is applied to locate the peak at the same frequency with MD results, but this amount of difference is not the origin of the trend itself and the value is not differed a lot compared to the initial guess from empirical formulation. The fitting results for other SWNTs are included in Supporting Material C [43].

Table 2. Simulation results for various aspect ratio.

	Num. of Atom	r^2/L (nm)	Temp. (K)	C_0	c_1	Γ_0	E (TPa)
(5,5)	400	0.23	50	0.10	0.004	$3.75\text{x}10^{-5}$	1.81
			100	0.16	0.006	$5.72\text{x}10^{-5}$	1.83
			300	0.10	0.010	$4.52\text{x}10^{-4}$	1.99
	480	0.20	50	0.08	0.004	$1.08\text{x}10^{-4}$	2.03
			100	0.10	0.006	$1.41\text{x}10^{-4}$	2.05
			300	0.06	0.010	$3.94\text{x}10^{-4}$	2.20
	560	0.17	50	0.05	0.005	$7.65\text{x}10^{-5}$	2.06
			100	0.05	0.006	$1.21\text{x}10^{-4}$	2.10
			300	0.05	0.011	$5.07\text{x}10^{-5}$	2.44
	660	0.15	50	0.04	0.005	$1.17\text{x}10^{-5}$	2.00
			100	0.04	0.007	$8.30\text{x}10^{-5}$	2.00
			300	0.05	0.012	$5.71\text{x}10^{-4}$	2.60
	820	0.11	50	0.02	0.006	$1.30\text{x}10^{-5}$	2.26
			100	0.02	0.008	$5.17\text{x}10^{-6}$	2.40
			300	0.03	0.014	$5.72\text{x}10^{-4}$	3.63
(10,10)	1320	0.60	50	0.40	0.002	$-1.44\text{x}10^{-4}$	1.48
			100	0.40	0.002	$-1.27\text{x}10^{-4}$	1.51
			300	0.40	0.004	$1.61\text{x}10^{-4}$	1.57
	4000	0.19	50	0.07	0.003	$-5.16\text{x}10^{-5}$	1.93
			100	0.06	0.004	$-2.14\text{x}10^{-4}$	2.05
			300	0.06	0.008	$5.02\text{x}10^{-5}$	2.09
(20,20)	8000	0.78	50	0.65	0.001	$-5.14\text{x}10^{-5}$	1.50
			100	0.65	0.001	$-3.70\text{x}10^{-5}$	1.54
			300	0.65	0.003	$1.35\text{x}10^{-4}$	1.63

4-2. Empirical formula

Interestingly, the value of C_0 shows a linear tendency in log-log scale following a kind

of aspect ratio. The trend approximately follows a $r^2 / r_0 L$ trend. r_0 is its bond length, which is included for non-dimensionalization. Regardless of the temperature difference, the value of C_0 follows the empirical formulation $C_0 = 0.25\left(\frac{r^2}{r_0 L}\right)^{1.7}$ in Fig. 8. The suspended case also shows similar tendency, but C_0 is a little larger than in the cantilevered cases, $C_0 = \left(\frac{r^2}{r_0 L}\right)^{1.7}$. This formulation is applied to the comparison with the experimental case as shown in Fig. 9.

4-3 Boundary condition

The boundary rigidity condition, such as slacking, has been reported as the reason of frequency shift of the multiple resonances in suspended FET system [33,45]. For this reason, the rigidity controlled by LJ potential function is also examined to check the role of boundary condition to the multiple resonances in case of free thermal vibrations. The perfectly rigid condition, denoted as “rigid”, is also calculated. All simulation conditions with LJ potentials constants for different rigidity are shown in Table S2.

The amplitude of each condition does not show any significant difference for each case, but only the value of C_0 differs over 2 times between the soft boundary and the rigid boundary case. The result is shown in the Table S5 of Supporting Material A [43]. The dependency of multiple resonances on the rigidity of boundary condition corresponds well with the results obtained with slacking [33] and further physical meaning is discussed in Sec 4-5.

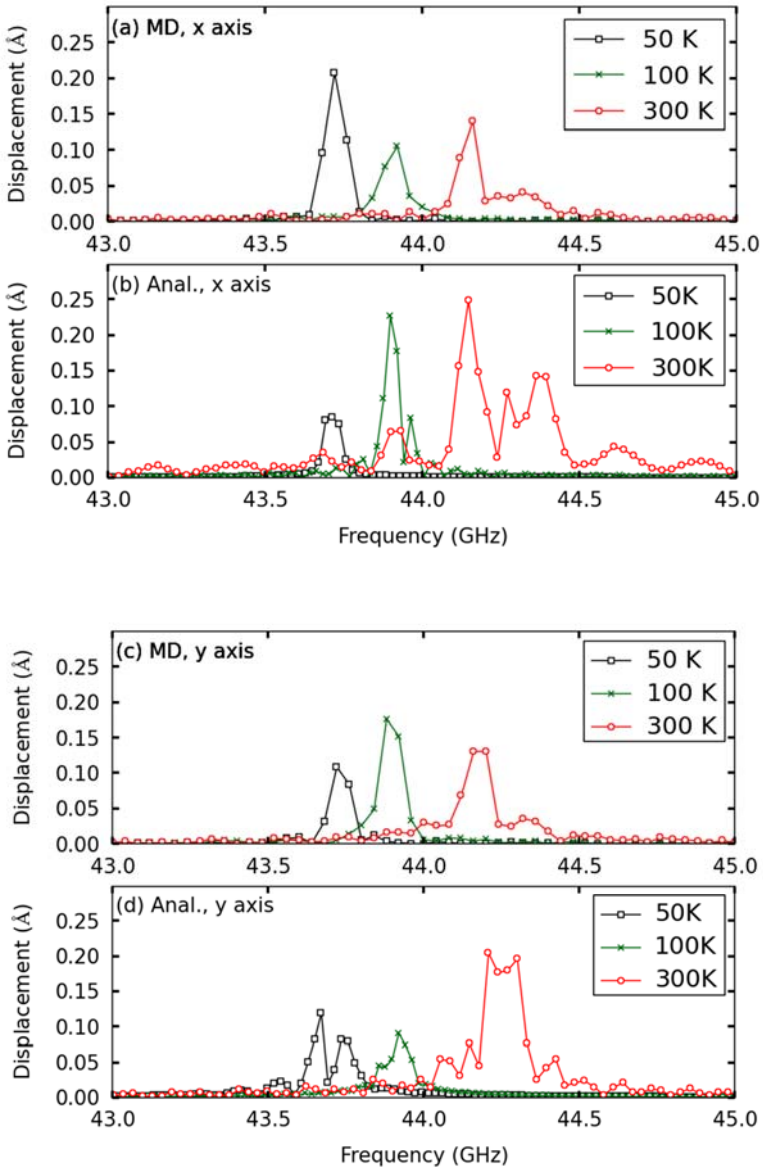

Fig. 7. Frequency response of 1st transverse mode of analytic solution and MD result along x and y axis, black line is 50 K, green line is 100 K and red line is 300 K of (5,5) 7.6 nm case: (a) MD simulation along x axis, (b) Analytical solution along x axis, (c) MD simulation along y axis, (c) Analytical solution along y axis.

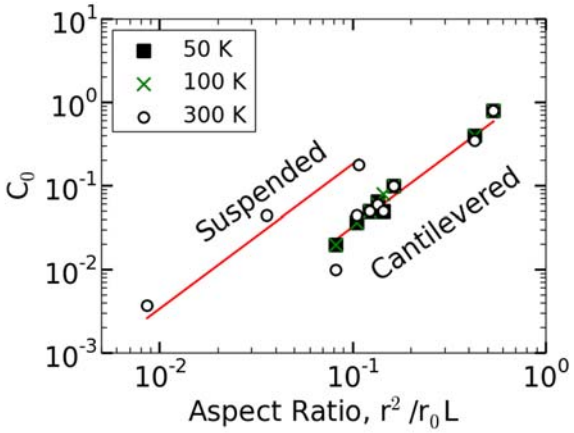

Fig. 8. C_0 plot of the results from 50 K (square), 100 K (cross) and 300 K (hollow circle) for cantilevered and suspended case with fitted result.

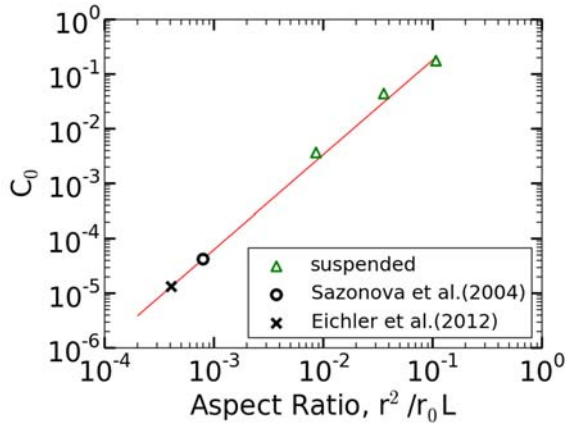

Fig. 9. C_0 fitting for comparison with experimental results for Eichler et al. [10](cross) and Sazonova et al. [18] (circle) and triangle is MD result with suspended SWNT.

4-4. Frequency response with discretized peaks

The last term in Eq. (5) and Eq. (6) has a square wave shape, which is rougly the

superposition of harmonics of its frequency components as below:

$$\tan^{-1}\left(-\frac{\sqrt{1-C_0^2}}{C_0}+\frac{1}{C_0}\tan\left(\frac{qC_0c_1^2}{4\omega}\tau\right)\right) \cong \frac{4}{\pi}A\left(\sin(2\pi f_1\tau)+\frac{1}{3}\sin(6\pi f_1\tau)+\frac{1}{5}\sin(10\pi f_1\tau)+\cdots\right) \tag{7}$$

,here, $f_1=\frac{qC_0c_1^2}{4\omega}$. The frequency response, $\hat{\omega}(f)$ for $\xi(\tau)\cong a(\tau)\cos(\omega\tau+\theta(\tau))$ becomes as below:

$$\hat{\omega}(f)=\int a(\tau)\sin(\omega\tau+\theta(\tau))\cdot e^{-i(2\pi f\tau)}\,d\tau \tag{8}$$

where,

$$a(\tau)\cong \text{Const.}+\text{Re}(e^{ic/\omega\tau}) \tag{9}$$

$$\sin(\omega\tau+\theta(\tau))\cong \text{Re}\left(e^{i\left(\omega\tau+\omega^*\tau+2\pi f_1\tau+6\pi f_1\tau+\cdots\right)}\right) \tag{10}$$

From this rough expression, one can easily assumed that the result of $\hat{\omega}(f)$ will have discrete frequency component for each harmonic frequency $\omega+\omega^*+\sum n\pi f_1$, where n is the harmonic number at Eq. (7) and $\omega*$ is for the rest of the terms in Eq. (5) or Eq. (6).

$f_1=\frac{qC_0c_1^2}{4\omega}$ is about 0.01 GHz for (5,5) 7.6 nm length at 300 K.

4-5. Clamping instability

Recently, the slacking at the boundary of suspended SWNT FET system is reported as the reason for resonance frequency shift dependent on temperature [31, 44]. Interestingly, such resonance frequency condition is also observed with cantilevered SWNT as shown in Fig. 10.

The (5,5) SWNT with 7.6 nm and 23.5 nm length is calculated with temperature from 50 K to 800 K. The resonance frequency is slightly increased until 300 K and experiences a rapid drop after 300 K. This temperature dependence is very similar to the results presented by Aykol et al. [44] from a suspended SWNT FET system. Alternation of rigidity conditions using the LJ potential function did not reveal any significant change in properties such as this temperature dependence.

The slight increase until 300 K is well described by the analytical solution, however, the later elasticity softening at temperatures higher than 300 K is not explainable with the same theory. Unlike the suspended fixation, however, resonance frequency shift of the cantilevered SWNT system can not be from the boundary rigidity nor thermal expansion. We suspect that the elastic modulus change from anharmonic force constants of the C-C bond may contribute to the shift with the larger amplitude of free thermal motion as the temperature increases.

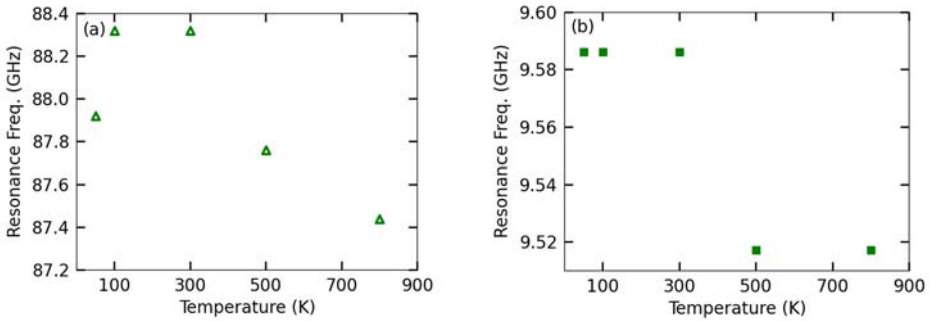

Fig. 10. Resonance frequency change for each temperature in MD simulation; (a) Cantilevered SWNT (5,5) 7.6 nm, (b) Cantilevered SWNT (5,5) 23.5 nm.

5. Frequency response in experiments

5-1. Frequency response of FET system

The approximate analytical solution and its parameters are applied to the experimental results for suspended FET systems using extrapolation as shown in Fig. 9. The signal from

those experiments is measured during the time when the tube is under the forced excitation in the resonance frequency range. Although the analytical solution in Eq. (3)~(6) is for free vibration, the comparison of frequency responses from experimental result is important to recognize the frequency response change by dissipative coupling. The difference of free vibration and forced excitation will give some clue of damping process of molecular systems.

The thermal expansion is simply ignored and c_1 is adapted from the Gibbs-Boltzamnn distribution. The Young's modulus starts from the empirical formulation [46] and is adjusted to make the peak locations matched with experimental result. Lastly, the value of C_0 is decided with the empirical formulation, $C_0 = \left(\frac{r^2}{r_0 L} \right)^{1.7}$.

a) 50 mK

The amplitude, c_1 from Gibbs-Boltzmann distribution at Fig. 11 (a) makes very narrow distance between peaks, so the similar frequency response to the experiment could be achieved with the amplitude at 1 K [6]. In Fig. 11 (b), the location of peaks is consistent with experimental data measured at 50 mK by Eichler et al. The experiment has external excitation so larger amplitude than its free thermal vibration is very natural.

If the motion is smaller than 50 mK, such as under 30 mK, [5] observing the peak separation becomes progressively more difficult due to its very low beating frequency which is proportional to the square of the amplitude. It is also possible that the only allowed planar motion could be near the ground state, in which case measuring beating signal is meaningless.

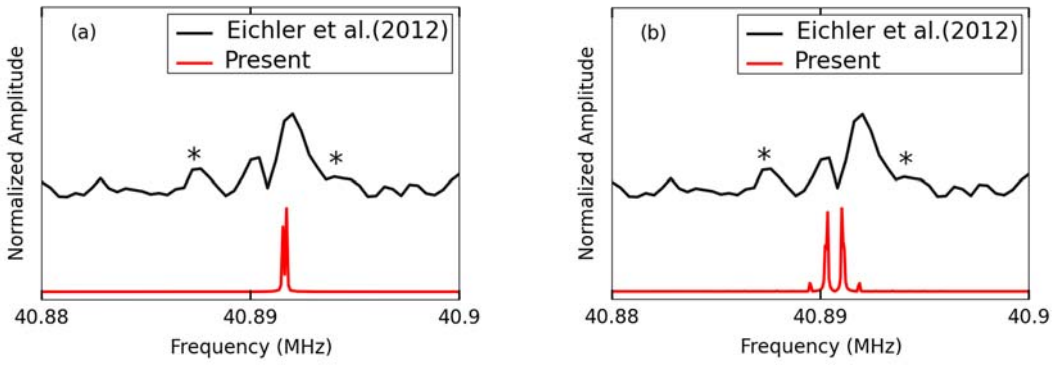

Fig. 11. Comparison of frequency response from the result of Eichler et al. [6] (black line, upper) and from analytic solution (red line, lower): The suspended CNT with L=2 μm and diameter = 1.5 nm with thickness 0.0706 nm. Fitting parameters are in Table 3.4. * mark represents the peak from noise; (a) with the amplitude from free thermal motion at 50 mK, (b) with the amplitude at 1 K.

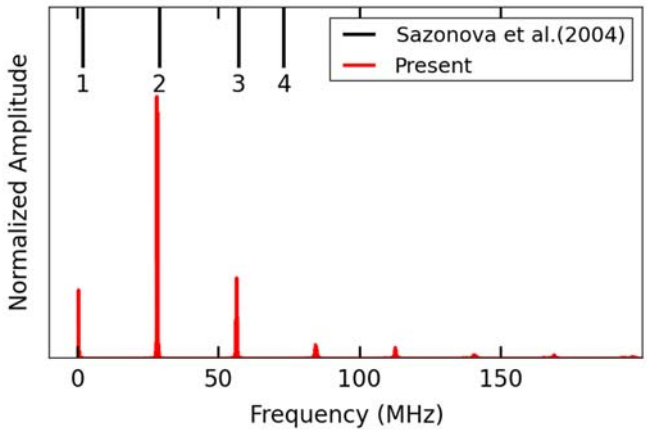

Fig. 12. Comparison of frequency response from the experiment done by Sazanova et al. [18] (black) and that from analytic solution (red): The suspended CNT with L=1.75 μm and diameter = 1 nm. Parameter for analytic solution is in Table 3.4.

b) Room temperature

We also checked another frequency response at 300 K with other experimental conditions. The location of peaks and numbers are in very close agreement as shown in Fig. 12 [18]. The very discrete peak distribution is comes directly from the phase function, which has a square wave shape in Eq. (5)~ (6). More precise explanation is in Section 4-4.

The frequency response from free vibration, having the same peaks as under forced conditions means that the damping process is not the main cause of peak separation, but the frequency response has to have multiple peaks because the vibration energy of suspended SWNT producing a beating signal from mode coupling due to its two degrees of freedom. The Fig. 11 and Fig. 12, therefore, indicate the possible existence of the periodic order of planar and non-planar motion with sudden change of phase in experiments and provide a reasonable explanation of multiple resonances as a part of natural resonance not directly from the nonlinear damping. The nonlinearity of free vibration of SWNT might be able to give a new viewpoint about the energy dissipation process in a quasi 1D system, describing how the 1st transverse mode is losing energy while the mechanical motion in the two orthogonal planes are interacting during the forced excitation.

6. Summary and discussion

In this work, we have compared the analytical model from the Green Lagrange strain tensor with the 1st order cantilever motion of SWNT using MD simulation and applied the same formulae to the simulation with the suspended boundary condition for the comparison with experimental results. An analytical solution to nonlinear bending vibrational mode shows the same characteristics as in molecular dynamic simulation such as 1) motion

exchange from planar to non-planar, 2) inversion of rotational direction and 3) frequency shift and peak separation rather than broadening. All of these characteristics are strongly dependent on the amplitude of the vibrational mode. Conventionally, the phase velocity of elastic waves does not depend on with the magnitude of the wave vector [47], but it is revealed that the nonlinear mechanical motion allows such condition in this study. The comparison in frequency domain shows that the interplay between the displacements of two transverse waves in orthogonal axes of the SWNT system is the main contribution of peak broadening, as predicted by Green function theory [9].

Q factor has important meaning to the relaxation time and SNR (signal to noise ratio) for sensory system. Since the multiple resonance peaks due to the degree of freedom of motion are inevitable, Lorentzian fitting for Q factor should be reconsidered for the system using the resonance of cantilevered or suspended bar set-up. Relaxation time is the duration to change the vibrational phase in steady state. So the presence of multiple peaks from the square wave shape like phase reverse as mentioned in Sec. 4-4 can give very direct duration of such using Eq. (7). In case of SNR, the multiple peaks are the result of 1st mode-1st mode interaction. The separated peaks, therefore, is hard to consider as the result of other modes interaction. The influence of 1 st mode and other higher order modes should be revealed first for SNR.

From good agreements in simulation and experiment, we can conclude that the equation of motion from strain energy simulation is capable of describing the mode coupling in macroscopic motion of molecular dynamic conditions, and its dependence on temperature and aspect ratio.

The reason why the governing equation from strain energy can be a common feature linking continuum mechanics and molecular systems, is presumably that the molecule, SWNT, has structural entanglement inducing anharmonicity, which can be interpreted into the strain energy of continuum mechanics. More precisely, the definition of the strain

includes the square of the displacements in two orthogonal axes at the same time so that the nonlinear terms of these variables possibly represent the interacting process as some sort of anharmonic force terms.

Further steps should build a theoretical connection between the anharmonicity and strain function for a better explanation of the relation between temperature and the motion exchange expressed by C_0, which controls beating frequency and peak span. The mechanism leading to the dependence of C_0, on the aspect ratio and rigidity of fixation will show more precise process of mode-mode interaction as dissipative coupling.

AUTHOR INFORMATION

Corresponding Author

Email: maruyama@photon.t.u-tokyo.ac.jp

Department of Mechanical Engineering, The University of Tokyo, 7-3-1 Hongo, Bunkyo-ku, Tokyo 113-8656, Japan

ACKNOWLEDGMENT

A part of this work was financially supported by Grants-in-Aid for Scientific Research (22226006, 25107002) and IRENA Project by JST-EC DG RTD, Strategic International Collaborative Research Program, SICORP. We also acknowledge supports from 'Global Center for Excellence for Mechanical Systems Innovation (The University of Tokyo). We thank Dr. A. Eichler for kindly providing the data for Fig. 11.

REFERENCES

[1] J. Chaste, A. Eichler, J. Moser, G. Ceballos, R. Rurali, A. Bachtold, Nat. Nanotechnol., 7, 301–4 (2012).

[2] J. Moser, J. Güttinger, A. Eichler, M. J. Esplandiu, D. E. Liu, M. I. Dykman, A. Bachtold, Nat. Nanotechnol., 8, 493–6 (2013).

[3] Y. Tao, J. M. Boss, B. A. Moores, C. L. Degen, Nat. Commun., 5, 3638 (2014).

[4] K. Kim, K. Jensen, and A. Zettl, Nano Lett. 9, 9, 3209-3213 (2009).

[5] J. Moser, A. Eichler, J. Güttinger, M. I. Dykman, A. Bachtold, Nat. Nano., 9, 1007–1011 (2014).

[6] A. Eichler, J. Moser, J. Chaste, M. Zdrojek, I. Wilson-Rae, A. Bachtold, Nature Nano., 6, 339–332 (2011).

[7] V. P. Adiga, R. De Alba, I. R. Storch, P. A. Yu, B. Ilic, R. A. Barton, S. Lee, J. Hone, P. L. McEuen, J. M. Parpia, and H. G. Craighead, Appl. Phys. Lett., 103, 14, 143103 (2013).

[8] A. Benyamini, A. Hamo, S. V. Kusminskiy, F. von Oppen, S. Ilani, Nat. Phys., 10, 151–156 (2014).

[9] A. De Martino, R. Egger, A. O. Gogolin, Phys. Rev. B, 79, 205408 (2009).

[10] H. Askes, E. C. Aifantis, Int. J. Solids Struct., 48(13), 1962–1990 (2011).

[11] D. Qian, G. J. Wagner, W. K. Liu, M. F. Yu, R. S. Ruoff, Appl. Mech. Rev. 55, 495–533 (2002).

[12] R. S. Ruoff, D. C. Lorentz, Carbon, 33, 925–930 (1995).

[13] M. M. J. Treacy, T. W. Ebbesen, J. M. Gibson, Nature, 381, 678-680 (1996).

[14] A. Krishnan, E. Dujardin, T. W. Ebbesen, P. N. Yianilos, M. M. J. Treacy, Phys. Rev. B, 58, 20, 14013-14019 (1998).

[15] B.I. Yakobson, C.J. Brabec, J. Bernholc, Phys. Rev. Lett., 76, 14, 2511–2514 (1996).

[16] Y. Huang, J. Wu, K. C. Hwang, Phys. Rev. B, 74, 245413 (2006).

[17] C. H. Chang, D. Okawa, H. Garcia, A. Majumdar, A. Zettl, Phys. Rev. Lett., 99, 045901 (2007).

[18] V. Sazonova, Y. Yaish, H. Ustünel, D. Roundy, T. A. Arias, P. L. McEuen, Nature, 431, 284–287 (2004).

[19] K. Jensen, K. Kim, A. Zettl, Nature Nano., 3, 533–537 (2008).

[20] S. Perisanu, P. Vincent, A. Ayari, M. Choueib, S. T. Purcell, M. Bechelany, D. Cornu, Appl. Phys. Lett., 90, 043113 (2007).

[21] E. Gil-Santos, D. Ramos, J. Martinez, M. F.-Regulez, R. Garcia, A. S. Paulo, M. Calleja, J. Tamayo, Nature Nano., 5, 641-645 (2010).

[22] S. Sawano, A.Takayuki, S. Akita, Nano Lett., 10, 3395–3398 (2010).

[23] X. Zhang, M. Hu, D. Poulikakos, Nano Lett., 12, 3410–3416 (2012).

[24] S. M. Carr, W. E. Lawrence, M. N. Wybourne, Physica B: Cond. Matt., 317, 464–467 (2002).

[25] M. Born, K. Huan, Dynamical Theory of Crystal Lattices, Oxford Univ Press (1954).

[26] M. Zhou, Proc. R. Soc. Lond. A, 459, 2347–2392 (2003).

[27] M. Arroyo, T. Belytschko, J. Mech. Phys. Solids, 50, 1941-1977 (2002).

[28] E. H. Feng, R. E. Jones, Phys. Rev. B, 81, 125436 (2010).

[29] E. H. Feng, R. E. Jones, Phys. Rev. B, 83, 195412 (2011).

[30] H. W. Ch. Postma, I. Kozinsky, A. Husain, M. L. Roukes, Appl. Phys. Lett., 86, 223105 (2005).

[31] A. W. Barnard, V. Sazonova, A. M. van der Zande, P. L. McEuen, PNAS, 2011, 109(47), 19093-6.

[32] I. Wilson-Rae, R. A. Barton, S. S. Verbridge, D. R. Southworth, B. Ilic, H. G. Craighead, J. M. Parpia, Phys. Rev. Lett., 106, 047205 (2011).

[33] H. Ustünel, D. Roundy, T. A. Arias, Nano Lett., 5, 3, 523–6 (2005).

[34] W. G. Conley, A. Raman, C. M. Krousgrill, S. Mohammadi, Nano Lett., 8, 1590–1595 (2008).

[35] A. Behboud, R. A. Scott, J. Sound Vib., 152(1), 183-188 (1992).

[36] I. Wilson-Rae, Phys. Rev. B, 77, 245418 (2008).

[37] S. J. Stuart, A. B. Tutein, J. A. Harrison, J. Chem. Phys., 112, 6472 (2000).

[38] S. J. Plimpton, J. Comput. Phys., 117, 1–19 (1995).

[39] T. Schneider, E. P. Stoll, R. Morf, Phys. Rev. B, 18, 1417–1424 (1978).

[40] S. Nosé, Mole. Phys., 52, 2, 255–268 (1984).

[41] S. Maruyama, Microscale Therm. Eng., 7, 41–50 (2003).

[42] P. Yi, D. Poulikakos, J. Walther, G. Yadigaroglu, Intern. Journ. of Heat and Mass Transfer, 45, 2087–2100 (2002).

[43] See Supporting material at http:// . The movie of nonlinear motion of SWNT and specific simulation conditions and results in frequency domain are presented.

[44] C.-H. Ho, R. A. Scott, J. G. Elsley, J. Sound Vib., 47, 333–339 (1976).

[45] M. Aykol, B. Hou, R. Dhall, S.-W. Chang, W. Branham, J. Qiu, S. B. Cronin, Nano Lett., online (2014).

[46] L.V. Zhigilei, C. Wei, D. Srivastava, Phys. Rev. B, 71, 165417 (2005).

[47] J. M. Ziman, (1960). Electrons and Phonons. OXFORD, University Press Inc., New York.

[48] P. K. Schelling, P. Keblinski, Phys. Rev. B, 035425 (2003).